On the Mobility and Manipulability of General Multiple Limb Robots

Antonio Bicchi, Claudio Melchiorri, and Daniele Balluchi

Abstract—**In this paper, the analysis of the differential kinematics and manipulability measures of robotic systems comprised of multiple cooperating limbs is considered. The goals of this study can be articulated in four points. First, to enumerate the degrees of freedom of the manipulation system (*mobility* analysis). Second, to describe analytically all possible first-order differential motions of the system at a given configuration (*kinematic* analysis). Third, to evaluate in the velocity domain the functionality of a manipulation system, with respect to the task it is required to perform (*velocity manipulability* analysis). Finally, to calculate the bounds for the velocities achievable by the system, given bounds on the capabilities of joint actuators (*velocity workspace* analysis). The assumptions made on the robotic system are quite general, so that many complex devices (e.g., dextrous hands, legged vehicles, whole-arm manipulators etc.) can be dealt with in a unified and convenient framework.**

I. Introduction

MANY of the most promising and challenging future applications of robotics are expected to involve systems with more complex kinematics than current serial-linkage robot arms. In that broader class of robotic devices fall for example multiple robotic arms used for the coordinated manipulation of objects, and multi-limb robots such as dexterous hands, walking machines, etc. Several researchers addressed the specific problems of some of these systems; see for example [1]–[3] for cooperative arms, [4]–[6] for dextrous hands, and [7], [8] for legged vehicles. The general underlying structure of such systems is clearly the same, and as such it has been treated e.g. by [9].

In general, a manipulation system can be regarded as a collection of links and joints, each with given geometric description. Among the joints, there is a distinction between active joints (those that can be actuated directly), and passive joints (typically incorporated by kinematic constraints arising from contact). One of the links (the "object") is considered as the reference member. The aim of this paper is to study the relationship between differential motions of the active joints and those of the object, that plays the role of the end-effector of the manipulation systems, and whose motions are the ultimate control objective.

Manuscript received July 20, 1993; revised June 1994. This work is supported by *Progetto Finalizzato Robotica* CNR, Italy, Contracts no. 92.01079.PF67 and 92.01047.PF67 (University of Pisa), and no. 92.01044.PF67 (University of Bologna).

A. Bicchi and D. Balluchi are with DEIS, Dip. di Elettronica Informatica e Sistemistica, Università di Bologna, Italia.

C. Melchiorri is with the Centro "E. Piaggio" and D.S.E.A., Università di Pisa, Italia.

IEEE Log Number 9409079.

In detail, the goals of this study can be articulated in four points. First, to enumerate and classify the degrees of freedom of the manipulation system (*mobility* analysis). Second, to describe analytically all possible first-order differential motions of the system at a given configuration (*kinematics* analysis). Third, to evaluate the functionality of a manipulation system, in a given configuration, with respect to the tasks it is required to perform in the velocity domain (*manipulability* analysis). Finally, to calculate the bounds for the velocities achievable by the system, given bounds on the velocities of joint actuators (*velocity workspace* analysis).

The analysis of these problems has not been solved, to our knowledge, in the general setting that is considered here. In particular, the kinematic analysis of cooperating robotic systems has been based on the assumption that every single arm has as many degrees of freedom as necessary to achieve arbitrary position/orientation in its task space. However, this assumption is not always verified in practical applications of cooperating manipulation. Such is the case, for instance, when common industrial manipulators with 3 or 4 joints are used together for tasks involving heavy loads or accurate positioning. A more recently developed application of cooperation between devices with "defective" kinematics is encountered in the analysis of *whole-limb* manipulation. This style of manipulation, that uses any link (in particular, including *proximal* links) of the limbs, is very common in nature, since it can provide more robust hold or more versatile motion in animal grasping and locomotion. The concept has been recently borrowed by roboticists: examples of such devices are the Whole-Arm Manipulator "WAM" developed at MIT, [10], the "DIGIT" system of Ohio State University, [11], or the whole-hand system "UB Hand-II" of the University of Bologna, [12].

The paper is organized as follows. In Section II, after introducing the notation and basic equations, the mobility and kinematics analysis of cooperating multi-limb manipulation is described, following the approach presented in [13]. In Section III this approach is applied for extending manipulability indices to general multiple robots, while Section IV describes the cooperative velocity workspaces. Section V discusses some case studies, and concluding comments are reported in Section VI.

II. Mobility and Differential Kinematics Analysis

We consider a general cooperating system, consisting of an arbitrary number of limbs and of an object that may be in contact with some or all of the links of the limbs. No

distinction is made whether the contacting links are at the extremities of the limb or not. Different contact models may be used to describe the interactions that take place between the limbs and the object [4]. Among these, the most important probably are the point-contact-with-friction model (or "hard-finger"), where only forces can be exerted at the contacts; the "soft-finger" model, that also allows torques about an axis normal to the surfaces to be applied; and the complete-constraint model (or "very-soft-finger"), where both forces and arbitrary torques can be applied. The kinematic constraints imposed by the ith contact can be explicited in terms of the relative velocities of two reference frames ${}^{o}C_i$ and ${}^{m}C_i$ both having the origin at the ith contact point $\mathbf{c}_i$, and fixed to the object and to the robot link, respectively. Let ω be the angular velocity of the manipulated object, and $\mathbf{v}$ the linear velocity of a reference point fixed with the object, both expressed in base frame. Choose the object reference point to coincide with the origin of base frame at the instant being considered. The linear and angular velocity (expressed in base frame) of ${}^{o}C_i$ can be written as

$$\begin{aligned} {}^{o}\dot{\mathbf{c}}_i &= \mathbf{v} + \omega \times \mathbf{c}_i; \\ {}^{o}\omega_i &= \omega. \end{aligned} \tag{1}$$

or, juxtaposing all such expressions for the n contact points in matrix notation, as

$${}^{o}\dot{\mathbf{x}} = \mathbf{G}^T \dot{\mathbf{u}}, \tag{2}$$

where $\dot{\mathbf{u}}$ is a 6-dimensional "twist" vector, ${}^{o}\dot{\mathbf{x}}$ is a $6n$-vector of velocities of the ${}^{o}C_i$ frames, and $\mathbf{G}$ is the $6 \times 6n$ *grasp* matrix. Explicit definition of these quantities is given in Appendix A. Analogously, the linear and angular velocities of frame ${}^{m}C_i$ corresponding to joint velocities $\dot{\mathbf{q}}$ can be written in compact form as

$${}^{m}\dot{\mathbf{x}} = \mathbf{J}\dot{\mathbf{q}}. \tag{3}$$

where $\mathbf{q}$ is an r-vector of joint coordinates, ${}^{m}\dot{\mathbf{x}}$ is a $6n$-vector of velocities of the ${}^{m}C_i$ frames, and $\mathbf{J}$ is the $6n \times r$, "Jacobian" matrix (see Appendix A).

Assuming a rigid-body model of the object and links of manipulators, the kinematic constraints imposed by contacts can be expressed as

$$\mathbf{H}({}^{o}\dot{\mathbf{x}} - {}^{m}\dot{\mathbf{x}}) = 0 \tag{4}$$

where $\mathbf{H}$ is a selection matrix of suitable size $(t \times 6n)$ that takes into account the type of contact and whose construction is described in Appendix A. It is worth pointing out that (4) models bilateral constraints, although unilateral or conic contact constraints are usually in effect for, e.g., the hard and soft finger contact models. This simplification is permitted, however, in the assumption that the system of forces grasping the object is *force closure*, ensuring that grasping forces can always be exerted on the object such that both balance equations and contact force constraints are not violated. A method for controlling grasping forces so as to avoid the violation of contact constraints in general cooperating mechanisms has been discussed in [14].

Substituting (2) and (3) in (4), directly we have

$$\mathbf{H}\mathbf{G}^T\dot{\mathbf{u}} - \mathbf{H}\mathbf{J}\dot{\mathbf{q}} = \mathbf{Q}\begin{bmatrix}\dot{\mathbf{u}} \\ \dot{\mathbf{q}}\end{bmatrix} = 0, \tag{5}$$

where $\mathbf{Q} \stackrel{\text{def}}{=} [\mathbf{H}\mathbf{G}^T - \mathbf{H}\mathbf{J}]$ is a $t \times (6 + r)$ matrix. Let $\mathbf{C}$ be a $(6 + r) \times m$ matrix whose columns form a basis of the m-dimensional null space of $\mathbf{Q}$, and partition it as $\mathbf{C} = [\mathbf{C}_1^T \ \mathbf{C}_2^T]^T$, where $\mathbf{C}_1$, and $\mathbf{C}_2$ are $6 \times m$, and $r \times m$ blocks, respectively.

The columns of $\mathbf{C}_1$ span the subspace of all possible rigid first-order differential motions of the object that do not break the contact constraints, and the columns of $\mathbf{C}_2$ span the corresponding subspace of joint motions. A complete description of the input-output relationship of a multiple-arm system can be obtained based on the two matrices $\mathbf{C}_1$ and $\mathbf{C}_2$. In fact, by applying column operations only and partitioning appropriately (see Appendix B), it is always possible to put the matrix $\mathbf{C}$ in the following form:

$$\begin{bmatrix}\mathbf{C}_1 \\ \mathbf{C}_2\end{bmatrix} = \begin{bmatrix}\mathbf{C}_{11} & \mathbf{C}_{12} & \mathbf{O} \\ \mathbf{O} & \mathbf{C}_{22} & \mathbf{C}_{23}\end{bmatrix} \tag{6}$$

where the columns of $[\mathbf{C}_{11} \ \mathbf{C}_{12}]$ form a basis of the range space of $\mathbf{C}_1$, denoted with $\mathcal{R}(\mathbf{C}_1)$, and the columns of $[\mathbf{C}_{22} \ \mathbf{C}_{23}]$ form a basis of $\mathcal{R}(\mathbf{C}_2)$. Therefore, we have that there exist some coefficient vectors $\mathbf{x}_1$, $\mathbf{x}_2$, and $\mathbf{x}_3$ (whose dimensions vary with the problem at hand) such that every possible pair of object velocities $\dot{\mathbf{u}}$ and joint velocities $\dot{\mathbf{q}}$ complying with the first-order kinematic and contact constraints of the multiple arm system can be written parametrically as

$$\begin{aligned} \dot{\mathbf{u}} &= \mathbf{C}_{11}\mathbf{x}_1 + \mathbf{C}_{12}\mathbf{x}_2 \\ \dot{\mathbf{q}} &= \mathbf{C}_{22}\mathbf{x}_2 + \mathbf{C}_{23}\mathbf{x}_3. \end{aligned} \tag{7}$$

A. Mobility Analysis

The mobility analysis of a cooperating manipulation system consists of the enumeration of the degrees of freedom of the overall mechanism and of its significant subsystems. In particular, we are interested in the evaluation of the connectivity, redundancy and indeterminacy of the system. The *connectivity* number N_c of cooperating linkages manipulating a common object has been defined in [4] as the minimum number of parameters required to specify the position and orientation of the object with respect to the base frame, subject to the kinematic and contact constraints of the system. The *redundancy* number N_r is defined as the minimum number of parameters required to specify the position and orientation of every link of the mechanism, when considering the object as fixed. The sum of the connectivity and redundancy numbers is the *mobility* N_m in the strict sense, [4]. Finally, the *indeterminacy* number N_i of a cooperating manipulation system is defined as the minimum number of parameters required to specify the position and orientation of the manipulated object with respect to the base frame, when all joints are locked.

Equation (7) and the structure of the block matrices in (6) contain the desired information on the mobility and kinematics

of general cooperating arms. Mobility analysis results can be summarized as follows:

- The mobility of the system is equal to the rank of the **C** matrix, i.e. $N_m = \mathrm{rank}(\mathbf{C})$;
- The connectivity of the system is equal to the rank of the $\mathbf{C}_1$ block, $N_c = \mathrm{rank}(\mathbf{C}_1)$ (and hence to the sum of the number of columns of $\mathbf{C}_{11}$ and $\mathbf{C}_{12}$);
- The indeterminacy of the system is equal to the number of columns of $\mathbf{C}_{11}$, $N_i = \mathrm{rank}(\mathbf{C}_{11})$;
- The redundancy of the system is equal to the number of columns of $\mathbf{C}_{23}$, $N_r = \mathrm{rank}(\mathbf{C}_{23})$.

With respect to previous results on the subject, by this method kinematic singularities of the linkages can be taken into account, thus providing exact results whereas the well-known formula of Kutzbach [15] (otherwise credited to Grübler [4]) would provide inequality relationships. More importantly, the proposed method allows not only the enumeration of the degrees of freedom, but also their kinematic description, as discussed below.

B. Differential Kinematics Analysis

More detailed kinematic information can also be elicited from (6):

- $\mathcal{R}(\mathbf{C}_{23})$ is the redundancy subspace of joint velocities that do not affect object velocities, but only modify the configuration of the manipulator limbs. Note that $\mathcal{R}(\mathbf{C}_{23}) = \mathcal{N}(\mathbf{HJ})$.
- $\mathcal{R}(\mathbf{C}_{11})$ is the indeterminacy subspace of object velocities that are left free by contact constraints. Note that $\mathcal{R}(\mathbf{C}_{11}) = \mathcal{N}(\mathbf{HG}^T)$.
- In the case that both $\mathbf{C}_{23}$ and $\mathbf{C}_{11}$ result empty ($N_i = N_r = 0$), there is a one-to-one correspondence between joint velocities in $\mathcal{R}(\mathbf{C}_{22})$ and object velocities in $\mathcal{R}(\mathbf{C}_{12})$, that can be written in parametric form as

$$\begin{cases} \dot{\mathbf{q}} = \mathbf{C}_{22}\mathbf{x} \\ \dot{\mathbf{u}} = \mathbf{C}_{12}\mathbf{x} \end{cases} \quad \forall \mathbf{x} \in R^{N_c}. \tag{8}$$

- In the case $N_i = 0$ and $N_r > 0$, any desired velocity of the object in the feasible subspace $\mathcal{R}(\mathbf{C}_{12})$ can be obtained by means of infinitely many combinations of joint velocities. From (7) we obtain

$$\dot{\mathbf{q}} = \mathbf{C}_{22}\mathbf{C}_{12}^{+}\dot{\mathbf{u}} + \mathbf{C}_{23}\mathbf{y}, \quad \forall \dot{\mathbf{u}} \in \mathcal{R}(\mathbf{C}_{12}), \tag{9}$$

where $\mathbf{y} \in R^{N_r}$ is a free coefficient vector. Any velocity $\dot{\mathbf{u}} \notin \mathcal{R}(\mathbf{C}_{12})$ can not be achieved by the system without breaking contact constraints. Note however that second- or higher-order differential motions in a forbidden direction may still be possible, see e.g. [16].

- In case N_i is not zero ($\mathbf{C}_{11}$ is not empty), the object velocity corresponding to a given joint velocity is not uniquely determined by the quasistatic analysis presented in this paper. In fact, from (7),

$$\dot{\mathbf{u}} = \mathbf{C}_{12}\mathbf{C}_{22}^{+}\dot{\mathbf{q}} + \mathbf{C}_{11}\mathbf{y}, \quad \forall \dot{\mathbf{q}} \in \mathcal{R}(\mathbf{C}_{22}). \tag{10}$$

where $\mathbf{y} \in R^{N_i}$ is a free coefficient vector. The indeterminacy can be solved or even exploited by taking into account the dynamics of the object, in a fashion similar to that presented by [17] for under-actuated mechanisms. This problem however falls beyond the scope of the present paper.

Example 1 (Part a): As an example of this technique, consider the simple case shown in Fig. 1, where a two-limb, four-link robot manipulates a spherical object. Note that a contact occurs between the object and the innermost link of the second limb, that only has one degree-of-freedom: hence, this is an instance of kinematically defective, whole-limb manipulation. Relevant dimensions and matrices are reported in Appendix C. Assuming hard-finger conditions at both contacts, and applying the above methods, for a generic configuration as that depicted in Fig. 1(a) we obtain the blocks of the partition (7) as

$$\mathbf{C}_{11} = \begin{bmatrix} 0 \\ 0 \\ -l_1 v \sin(q_1 - q_3) - u v \sin(q_1 + q_2 - q_3) \\ -L(l_1 \sin q_1 + u \sin(q_1 + q_2)) \\ L + v \cos q_3 - l_1 \cos q_1 - u \cos(q_1 + q_2) \\ v \sin q_3 - l_1 \sin q_1 - u \sin(q_1 + q_2) \\ 0 \end{bmatrix}$$

$$\mathbf{C}_{12} = \begin{bmatrix} -L(l_1 \sin q_1 + u \sin(q_1 + q_2)) v \sin q_3 & l_1 u v \sin q_2 \sin q_3 \\ L(l_1 \cos q_1 + u \cos(q_1 + q_2)) v \sin q_3 & -(L + v \cos q_3) l_1 u \sin q_2 \\ 0 & 0 \\ 0 & 0 \\ 0 & 0 \\ l_1 v \sin(q_1 - q_3) + u v \sin(q_1 + q_2 - q_3) & l_1 u \sin q_2 \end{bmatrix}$$

$$\mathbf{C}_{22} = \begin{bmatrix} l_1 v \sin(q_1 - q_3) + u v \sin(q_1 + q_2 - q_3) + L v \sin q_3 \\ 0 \\ L(l_1 \sin q_1 + u \sin(q_1 + q_2)) + l_1 v \sin(q_1 - q_3) \\ \quad + u v \sin(q_1 + q_2 - q_3) \\ 0 \end{bmatrix}$$

$$\begin{bmatrix} l_1 u \sin q_2 - u v \sin(q_1 + q_2 - q_3) - L u \sin(q_1 + q_2) \\ L(l_1 \sin q_1 + u \sin(q_1 + q_2)) + l_1 v \sin(q_1 - q_3) \\ \quad + u v \sin(q_1 + q_2 - q_3) \\ 0 \\ 0 \end{bmatrix}$$

$$\mathbf{C}_{23} = \begin{bmatrix} 0 \\ 0 \\ 0 \\ 1 \end{bmatrix}.$$

For $q_2 \neq \nu\pi$, $\nu = 0, 1, 2, \ldots$, the redundancy of the system is $N_r = 1$ (corresponding to the second link of the right limb not touching the object), and indeterminacy is $N_i = 1$: in fact, the object may instantaneously rotate, without violating contact constraints, about the axis through the contact points. Connectivity of the system is $N_c = 3$, and mobility is $N_m = 4$.

If either contact is soft-finger (i.e., rotations about the normal direction to the contact surface are prevented by friction), the indeterminacy is eliminated. In this case, $\mathbf{C}_{11}$ results empty while other blocks are unchanged, so that $N_i = 0$, $N_r = 1$, $N_c = 2$, and $N_m = 3$. If contacts are complete-constraint, the **C** matrix results empty. There are no possible

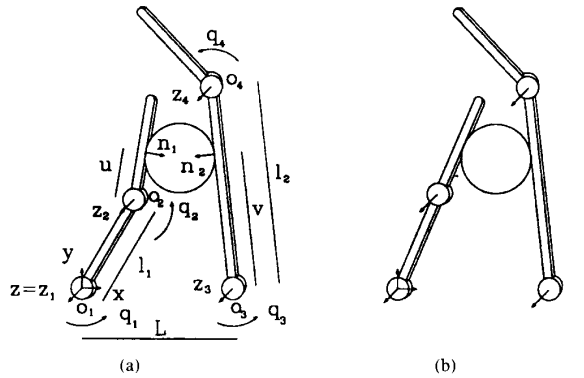

Fig. 1. Two limbs of a robot manipulating a spherical object. The limb on the right uses its inner phalanx to envelope the object. (a) generic configuration; (b) singular configuration.

motions for the robot in this case (as far as the rigid body model is maintained), as can be easily seen by inspection.

Singular configurations occur for $q_2 = 0$ or integer multiples of π, where the block $\mathbf{C}_{12}$ looses rank, see Fig. 1(b). With respect to the block description above, in the singular case $\mathbf{C}_{12}$ and $\mathbf{C}_{22}$ reduce to the first column, while the second column of $\mathbf{C}_{22}$ enters the block $\mathbf{C}_{23}$. Accordingly, the connectivity of the object is reduced to $N_c = 2$ ($N_c = 1$ for soft-fingers), while one redundant degree-of-freedom is gained in singular configurations beyond the trivial motion of joint 4 ($N_r = 2$).

III. Manipulability Velocity Ellipsoids

The motivation that led roboticists to develop manipulability analysis tools such as those considered in this section was to identify the configurations of the manipulation system that are more suitable for executing specific tasks, and to give a performance measure of the manipulation system in a given configuration. Salisbury and Craig [18] proposed to choose the configurations of the fingers of a robotic hand on the basis of their "isotropy," i.e. their ability to control forces in any direction with the same accuracy. The isotropy performance criterion can be conveniently expressed in mathematical terms using the condition number of the manipulator Jacobian matrix. Yoshikawa [19]–[21] extended the concept to a general description of the kineto-static capabilities of a single-arm robot by introducing the notion of *manipulability ellipsoids*. The velocity manipulability ellipsoid, for instance, defines the set of velocities (expressed in the task reference frame) that the end-effector can attain, when the joint velocities belong to a given subset of their space (in particular, to the unitary ball centered in the origin). The direction in task space corresponding to the longest axis of the velocity ellipsoid corresponds to the maximum amplification (or "mechanical advantage") of joint velocities. Analogous definitions are valid in the force domain. The isotropic condition is achieved when the ellipsoids are spherical. The ellipsoid approach provides a deep insight in the structure of the joint space/task space mappings, and allows the evaluation of the suitability of proposed robot configurations for a given task by direct comparison with a target "task ellipsoid" [6].

In its original version, the manipulability ellipsoid method can be applied to single-arm robots that have at least as many degrees of freedom as necessary to achieve arbitrary configurations in their task space. In this case, the mapping between joint space and task space velocities is defined by $\dot{\mathbf{u}} = \mathbf{J}\,\dot{\mathbf{q}}$. An inverse mapping can be expressed in terms of a generalized inverse of the Jacobian as $\dot{\mathbf{q}} = \mathbf{J}^{+}\dot{\mathbf{u}}$. The unit ball in joint velocity space, $\dot{\mathbf{q}}^T\dot{\mathbf{q}} \leq 1$, is mapped in the ellipsoid $\dot{\mathbf{u}}^T\mathbf{J}^{+T}\mathbf{J}^{+}\dot{\mathbf{u}} \leq 1$ in task space. Analogously, in the force domain, the mapping $\tau = \mathbf{J}^T\mathbf{w}$ is considered: the unit ball in the joint torque space, $\tau^T\tau \leq 1$, is mapped in the task space wrench ellipsoid $\mathbf{w}^T\mathbf{J}\mathbf{J}^T\mathbf{w} \leq 1$. It should be noted that, in general, it is necessary to introduce weighting of the input and output variables to preserve physical consistency of the expressions above [22]. The two ellipsoids share the same set of principal directions, while the lengths of their axes are reciprocal. Such directions and lengths are computed by means of a singular value decomposition of the Jacobian, $\mathbf{J} = \Phi\Sigma\Psi$: the principal axes of the velocity ellipsoid are given by $\Sigma_{11}\phi_1, \ldots, \Sigma_{nn}\phi_n$, where Σ_{ii} is the i-th singular value of $\mathbf{J}$, and ϕ_i is the corresponding column of Φ. Dually, the principal axes of the force ellipsoid are $\phi_1/\Sigma_{11}, \ldots, \phi_n/\Sigma_{nn}$.

Due to its potential usefulness in applications, attempts to extend the concept of manipulability ellipsoids to multiple-arm systems have been recently made. In [23] and [24] two different techniques are proposed, aimed at characterizing the kinetostatic capabilities of cooperating mechanisms in performing force/velocity targets in the task space. In particular, in [23] a manipulability velocity ellipsoid of a dual-arm system is defined by intersecting the ellipsoids pertaining to each arm considered as a single robot. In [24], a global approach is proposed that uses the grasp matrix $\mathbf{G}$ to define a composite "Jacobian" matrix for the whole system. Although useful in some cases, these two approaches fail when applied to systems with less than six degrees of freedom per cooperating limb. For a related discussion, see [25], [26] and the first case study in Section V.

As mentioned in the introduction, we are interested in extending the velocity manipulability analysis to a broader category of manipulation devices. Similarly to the classical approach proposed by Yoshikawa, our approach is based on an efficiency index defined as the ratio of an input effort and an output performance, for the robot in a given configuration. In fact, the input effort function for the system can be defined as a norm of the joint velocity vector, $\|\dot{\mathbf{q}}\|$, and, analogously, the output performance function as a norm of the object's velocity vector, $\|\dot{\mathbf{u}}\|$. Therefore, the performance-to-effort ratio

$$R_v \stackrel{\text{def}}{=} \frac{\|\dot{\mathbf{u}}\|}{\|\dot{\mathbf{q}}\|} \tag{11}$$

may be used as a measure of the efficiency of the system in a particular configuration. In accordance with the nature of manipulability ellipsoids, we specialize the norms above in *weighted 2-norms* as

$$\|\dot{\mathbf{q}}\| = \sqrt{\dot{\mathbf{q}}^T\mathbf{W}_q\dot{\mathbf{q}}};$$
$$\|\dot{\mathbf{u}}\| = \sqrt{\dot{\mathbf{u}}^T\mathbf{W}_u\dot{\mathbf{u}}},$$

where $\mathbf{W}_q$ and $\mathbf{W}_u$ are constant, symmetric, positive definite weighting matrices of suitable size and physical dimensions. Let us first reconsider the standard case of a single, nonredundant robot arm, for which the relation $\dot{\mathbf{u}} = \mathbf{J}\dot{\mathbf{q}}$ holds. Equation (11) may be rewritten as

$$R_v^2(\dot{\mathbf{q}}) = \frac{\dot{\mathbf{q}}^T \mathbf{J}^T \mathbf{W}_u \mathbf{J} \dot{\mathbf{q}}}{\dot{\mathbf{q}}^T \mathbf{W}_q \dot{\mathbf{q}}}. \tag{12}$$

As it is well known, the maximum (minimum) value of the *Rayleigh quotient* in (12) corresponds to the maximum (minimum) eigenvalue of the *pencil* $\mathbf{J}^T\mathbf{W}_u\mathbf{J} - \lambda\mathbf{W}_q$. Accordingly, the directions (in the joint space) in which a maximum (minimum) efficiency is obtained are given by the generalized eigenvectors corresponding to the maximum (minimum) eigenvalues of the pencil. Details on the efficient computation of generalized eigenvalues are reported e.g. in [28]. If $\lambda_{\max}$ is the maximum eigenvalue and $\dot{\mathbf{q}}_{\max}$ the corresponding eigenvector, the corresponding direction in the task space is given by $\mathbf{J}\dot{\mathbf{q}}_{\max}$. In the following we show that this simple reformulation of Yoshikawa's manipulability ellipsoids, associated with the mobility analysis discussed in Section II-A, lends itself to a very straightforward generalization to multiple manipulation systems.

Nonredundant Systems: Assume at first that the submatrices $\mathbf{C}_{11}$ and $\mathbf{C}_{23}$ are empty, see (8). Although the system may not have full mobility in task space, there is a one-to-one relation between the motions of the joints and of the object, i.e. there is neither indeterminacy nor redundancy. In this case, the performance-to-effort ratio is defined as

$$R_v^2 = \frac{\dot{\mathbf{u}}^T \mathbf{W}_u \dot{\mathbf{u}}}{\dot{\mathbf{q}}^T \mathbf{W}_q \dot{\mathbf{q}}} = \frac{\mathbf{x}^T \mathbf{C}_{12}^T \mathbf{W}_u \mathbf{C}_{12} \mathbf{x}}{\mathbf{x}^T \mathbf{C}_{22}^T \mathbf{W}_q \mathbf{C}_{22} \mathbf{x}}. \tag{13}$$

The maximum value of R_v corresponds to the maximum eigenvalue $\lambda_{\max}$ of the symmetric-definite pencil $\mathbf{C}_{12}^T\mathbf{W}_u\mathbf{C}_{12} - \lambda\mathbf{C}_{22}^T\mathbf{W}_q\mathbf{C}_{22}$. The corresponding generalized eigenvector $\mathbf{x}_{\max}$ gives the direction, in the parameter R^{N_c} space, where maximum performance are obtained. The corresponding directions in the task and joint velocity spaces are

$$\begin{aligned} \dot{\mathbf{u}}_{\max} &= \mathbf{C}_{12}\mathbf{x}_{\max} \\ \dot{\mathbf{q}}_{\max} &= \mathbf{C}_{22}\mathbf{x}_{\max}. \end{aligned} \tag{14}$$

Obviously, similar considerations apply for $\lambda_{\min}$, the minimum generalized eigenvalue, and $\mathbf{x}_{\min}$, the corresponding eigenvector. Note that by computing the generalized eigenvalues/eigenvectors of (13), an ellipsoid is described in $\mathcal{R}(\mathbf{C}_{12})$, the actual N_c-dimensional task space of the manipulation system at the given configuration.

Example 1 (Part b): Consider again the robot of Fig. 1, disregarding the second link of the right limb. Assuming soft-finger contacts, manipulation may be performed by rolling the object along the links. The robot task is to lower the object center along the y direction to reach a more "manipulable" configuration in order to prepare for a subsequent fine operation. Note that a task is chosen that is compatible with the kinematic constraints of the system, i.e. the desired object velocity $\dot{\mathbf{u}}_d$ must lie in the span of the columns of $\mathbf{C}_{12}$. The manipulation is then accomplished by solving $\dot{\mathbf{u}}_d = \mathbf{C}_{12}\mathbf{x}$ for $\mathbf{x}$ and commanding joint velocities $\dot{\mathbf{q}} = \mathbf{C}_{22}\mathbf{x}$. This control law, along with the equations of rolling reported in Appendix C.1, defines the differential equation of motion of the robot. Fig. 2 depicts four configurations of the robot during manipulation, while Fig. 3 reports plots of the relevant variables obtained by simulation. In Fig. 2, for each configuration the shape of the two-dimensional velocity manipulation ellipsoid in the 6-dimensional space of object velocities is reported. For clarity purposes, the plane spanned by the columns of $\mathbf{C}_{12}$ where the ellipses lie is represented onto the plane of motion of the robots.

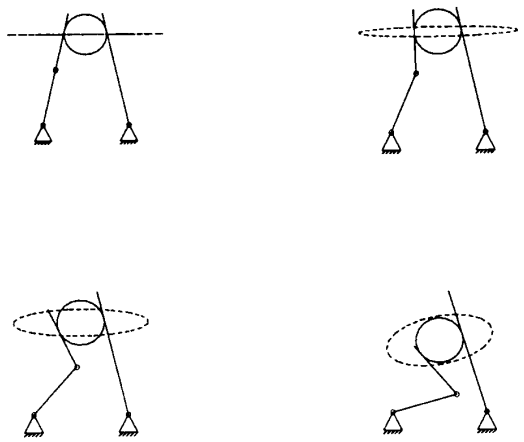

Fig. 2. Four configurations of the robot of example 1-b moving the object downward by rolling. Manipulability ellipsoids are superimposed, showing that more isotropic configurations are achieved.

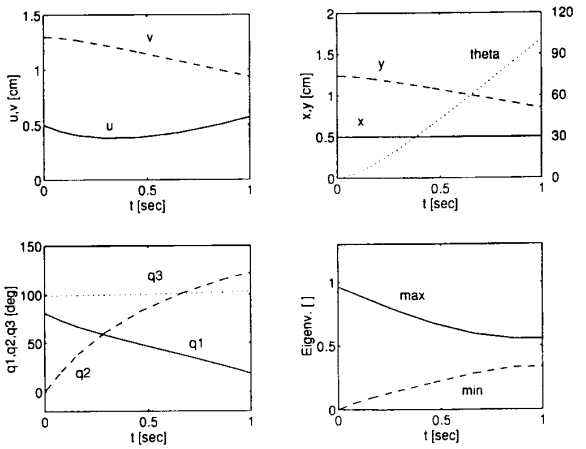

Fig. 3. Simulation results for the whole-limb manipulation of example 1-b.Upper left: contact coordinates u, v; Upper right: coordinates of the object; Lower left: joint angles; Lower right: generalized manipulability eigenvalues.

Redundant Systems: Assume now that the system has some degree of redundancy, i.e. there exist some combination of joint movements that do not generate any motion of the object. This fact reflects in the appearance of a nonempty submatrix $\mathbf{C}_{23}$, see (9). As a consequence, there is a degree of arbitrariness in the choice of joint motions to achieve given object motions. According to our definition of an input effort function, however, we will choose the joint motion that accomplishes the goal with minimum effort expendi-

ture. Therefore, we want to solve the following constrained optimization problem:

$$\arg\min_{\dot{\mathbf{q}}} \quad \dot{\mathbf{q}}^T\mathbf{W}_q\dot{\mathbf{q}}$$
$$\text{Subject to} \quad \begin{cases}\dot{\mathbf{q}} = \mathbf{C}_{22}\mathbf{x} + \mathbf{C}_{23}\mathbf{y} \\ \dot{\mathbf{u}} = \mathbf{C}_{12}\mathbf{x}\end{cases}$$

where $\mathbf{y} \in R^{N_r}$ is a free vector to be determined. By equating the gradient of $\dot{\mathbf{q}}^T\mathbf{W}_q\dot{\mathbf{q}}$ to zero it can be easily verified that the minimum is obtained for

$$\mathbf{y} = -(\mathbf{C}_{23}^T\mathbf{W}_q\mathbf{C}_{23})^{-1}\mathbf{C}_{23}^T\mathbf{W}_q\mathbf{C}_{22}\mathbf{x} \stackrel{\text{def}}{=} -\mathbf{C}_{23q}^+\mathbf{C}_{22}\mathbf{x}.$$

The corresponding optimal solution is

$$\begin{aligned}\hat{\dot{\mathbf{q}}} &= \mathbf{C}_{22}\mathbf{x} - \mathbf{C}_{23}\mathbf{C}_{23q}^+\mathbf{C}_{22}\mathbf{x} \\ &= (\mathbf{I} - \mathbf{C}_{23}\mathbf{C}_{23q}^+)\mathbf{C}_{22}\mathbf{x} \\ &\stackrel{\text{def}}{=} \hat{\mathbf{C}}_{22}\mathbf{x}.\end{aligned}$$

Therefore, the Rayleigh performance-to-effort quotient for redundant systems is written as

$$R_v^2(\mathbf{x}) = \frac{\mathbf{x}^T\mathbf{C}_{12}^T\mathbf{W}_u\mathbf{C}_{12}\mathbf{x}}{\mathbf{x}^T\hat{\mathbf{C}}_{22}^T\mathbf{W}_q\hat{\mathbf{C}}_{22}\mathbf{x}}. \tag{15}$$

Similarly to the previous case, if $\lambda_{\max}$, $\mathbf{x}_{\max}$ are the maximum generalized eigenvalue and the corresponding eigenvector of the associated pencil, the "optimal" velocity vectors are given by

$$\begin{aligned}\dot{\mathbf{u}}_{\max} &= \mathbf{C}_{12}\mathbf{x}_{\max} \\ \dot{\mathbf{q}}_{\max} &= \hat{\mathbf{C}}_{22}\mathbf{x}_{\max}.\end{aligned} \tag{16}$$

In the case of quasistatic indeterminacies in the manipulation system, the velocities of the object corresponding to given joint velocities can be completely determined only if the dynamics of the problem are taken into account. What we have in this case is an under-actuated mechanism, whose dynamics have been studied in some detail for example in [17], [29]. The discussion of the dynamical behavior of such systems is beyond the scope of this paper.

IV. Velocity Workspace Analysis

The manipulability ellipsoid method provides the directions in task space where the robot can attain maximum performance with a given effort. Although this is an important indication, it does not exhaust the designer's interest in describing the kinematic characteristics of the task space of a robot at different configurations. Another key point in characterizing the kinematics of manipulators has been pointed out by [30] and consists in describing the limits of performance in the velocity workspace corresponding to limitations of the input effort that joint actuators can provide. In general, such limitations impose that the operating points of the actuators lie within a given subset of the combined effort-velocity space. For actuators used most commonly in robotics, such as electric motors, this set is best approximated by a convex polytope (a region limited by planar facets). Such joint-space polytope is mapped by the linear differential kinematic relationship of the robot in a polytope in the robot force-velocity task space. Although the original formulation [30] of polytopes in combined force-velocity workspaces is intriguing, it falls beyond the scope of the present paper. In this section, the approach of [30] to describing velocity workspaces is generalized to general multiple limb robots.

A typical problem in the analysis of velocity workspaces is the determination of the task-space directions where the best output performance, in this case the maximum task space velocities, can be attained, provided that joint-space limitations of the form

$$\dot{q}_{i,\min} \le \dot{q}_i \le \dot{q}_{i,\max} \quad i = 1, \ldots, r \tag{17}$$

are in order. The possible asymmetry of bounds in (17) is notationally inconvenient, and can be eliminated by applying a suitable transformation of joint variables as

$$\mathbf{r} \stackrel{\text{def}}{=} \mathbf{D}\dot{q} + \mathbf{r}_o, \tag{18}$$

where

$$\mathbf{D} \stackrel{\text{def}}{=} \operatorname{diag}\left[\frac{2}{\dot{q}_{1,\max} - \dot{q}_{1,\min}}, \ldots, \frac{2}{\dot{q}_{r,\max} - \dot{q}_{r,\min}}\right],$$
$$\mathbf{r}_o \stackrel{\text{def}}{=} \left[-\frac{\dot{q}_{1,\max} + \dot{q}_{1,\min}}{\dot{q}_{1,\max} - \dot{q}_{1,\min}}, \ldots, -\frac{\dot{q}_{r,\max} + \dot{q}_{r,\min}}{\dot{q}_{r,\max} - \dot{q}_{r,\min}}\right]^T.$$

Thus, the polytope of bounds on input velocities is concisely described by $P_r' \stackrel{\text{def}}{=} \{\mathbf{r} \in R^r: \|\mathbf{r}\|_\infty \le 1\}$. If the output performance is measured by the weighted 2-norm of the object velocity $\dot{\mathbf{u}}$, the workspace analysis problem is equivalent to finding the direction in the velocity space that maximizes the quotient

$$R_r' = \frac{\|\dot{\mathbf{u}}\|_2}{\|\mathbf{r}\|_\infty}. \tag{19}$$

For single, nonredundant serial link manipulators, the problem is easily solved considering the input polytope P_r' and its mapping into the task space given by $\dot{\mathbf{u}} = \mathbf{J}\dot{\mathbf{q}}$. Since this mapping is linear in $\dot{\mathbf{q}}$, and since there is a one-to-one correspondence between points in joint and task velocity space, a polytope is defined in the task space, whose vertices are the image of the vertices of P_r'. Inspection of the vertices directly gives the desired maximum performance. The extension to the more general context considered in this paper is discussed in the sequel.

Nonredundant Systems: Consider first a manipulator with $N_i = N_r = 0$. The input bounding polytope is further restricted in this case by the kinematic constraints (8) to the intersection of P_r' with the affine linear manifold $\Pi \stackrel{\text{def}}{=} \{\mathbf{r} \in R^r: \mathbf{r} = \mathbf{D}\mathbf{C}_{22}\mathbf{x} + \mathbf{r}_o, \mathbf{x} \in R^{N_c}\}$. The intersection is a convex polytope P_r. A convex polytope P_x in R^{N_c} is also implicitly defined by $P_x \stackrel{\text{def}}{=} \mathbf{x} \in R^{N_c}: \|\mathbf{r}\|_\infty = \|\mathbf{D}\mathbf{C}_{22}\mathbf{x} + \mathbf{r}_o\|_\infty \le 1\}$. Since $\mathbf{D}$ is invertible and $\mathbf{C}_{22}$ is full column rank, every vertex of P_x is mapped in one and only one vertex of P_r. According to (8), P_x is mapped in a third polytope P_u in the task space by another bijection ($\mathbf{C}_{12}$ is full column rank). The latter polytope allows us to evaluate system performances. In fact, from the properties of norms and the convexity of P_u, it follows that maximum performance is attained along a direction pointing at a vertex of P_u. Thus, the desired direction of maximum performance in task space, and the corresponding

joint velocities, can be found by exhaustive search of the polytope vertices. An efficient algorithm for enumerating such vertices is as follows.

By introducing *slack variables* $\sigma \in R^{2r}$, inequality constraints on input velocities are transformed into a matrix equation as

$$\mathbf{A}\mathbf{z} = \mathbf{b}. \tag{20}$$

with

$$\mathbf{A} = \begin{bmatrix} \mathbf{DC}_{22} & \mathbf{I} \\ -\mathbf{DC}_{22} & \end{bmatrix}, \quad \mathbf{z} = \begin{bmatrix} \mathbf{x} \\ \sigma \end{bmatrix}, \quad \mathbf{b} = \begin{bmatrix} 1 - r_{o1} \\ \vdots \\ 1 - r_{or} \\ 1 + r_{o1} \\ \vdots \\ 1 + r_{or} \end{bmatrix}.$$

where $\mathbf{A}$ is a $2r \times (N_c + 2r)$ matrix whose rank is $2r$, $\mathbf{z} \in R^{N_c+2r}$, and $\mathbf{b} \in R^{2r}$. The set of solutions to (20) with the condition $\sigma_i \geq 0$, $i = 1, \ldots, 2r$ describes the polytope P_x. At the vertices of P_x, at least N_c slack variables are null.

Define an index set $\mathcal{I} = \{i_1, i_2, \ldots, i_{N_c}\} \subset \{1, 2, \ldots, 2r\}$. The number s of possible different sets $\mathcal{I}_k$, $k = 1, \ldots, s$, is: $s = \frac{2r!}{(2r-N_c)!N_c!}$. Consider the $2r \times 2r$ square matrix $\mathbf{B}_k$ obtained from $\mathbf{A}$ by deleting the N_c columns with indices $N_c + i$, $i \in \mathcal{I}_k$. Note that the first N_c columns of $\mathbf{A}$ are present in each of the $\mathbf{B}_k$ matrices. Such a construction of $\mathbf{B}_k$ amounts to imposing that solutions of (20) have components $\sigma_i = 0$, $i \in \mathcal{I}_k$. If $\mathbf{B}_k$ is invertible, a *basic solution* $\mathbf{z}_k = [(\mathbf{B}_k^{-1}\mathbf{b})^T, \mathbf{0}^T]^T$ of (20) is obtained. Invertibility of $\mathbf{B}_k$ can be efficiently checked by testing the rank of the $N_c \times N_c$ matrix whose elements are $\mathbf{A}_{ij}, i \in \mathcal{I}_k, j = 1, \ldots, N_c$. Among basic solutions, those with nonnegative $\sigma_j, j \notin \mathcal{I}_k$ (*feasible basic solutions*) contain the coordinates $\mathbf{x}$ of the vertices of P_x. At this point, P_u, P_r, and P_q (the polytope in joint velocity space), are directly evaluated by means of (18) and (8).

Example 1 (Part c): As an example of application of this technique, consider again the two-limb robot of Fig. 1. If soft-finger contacts are assumed, and disregarding the second joint of the right limb (i.e. $r = 3$), the kinematic analysis matrices evaluated at $q_1 = \pi/4$, $q_2 = \pi/4$, $q_3 = \pi/2$, $u = 0.5$, $v = 1$, are

$$\mathbf{C}_{12} = \begin{bmatrix} -1 & 0.25 \\ 0.5 & -0.25 \\ 0 & 0 \\ 0 & 0 \\ 0 & 0 \\ -0.5 & 0.25 \end{bmatrix}, \quad \mathbf{C}_{22} = \begin{bmatrix} 0.5 & -0.25 \\ 0 & 0.5 \\ 0.5 & 0 \end{bmatrix}.$$

and therefore $N_i = N_r = 0$, $N_c = 2$. Given the bounds on joint velocities (in [rad/sec])

$$\begin{aligned} -1.2 \leq \dot{q}_1 \leq 1 \\ -1 \leq \dot{q}_2 \leq 1 \\ -1 \leq \dot{q}_3 \leq 0.8 \end{aligned}$$

the terms of (20) are evaluated as

$$\mathbf{A} = \begin{bmatrix} 0.455 & -0.227 & 1 & 0 & 0 & 0 & 0 & 0 \\ 0 & 0.5 & 0 & 1 & 0 & 0 & 0 & 0 \\ 0.556 & 0 & 0 & 0 & 1 & 0 & 0 & 0 \\ -0.455 & 0.227 & 0 & 0 & 0 & 1 & 0 & 0 \\ 0 & -0.5 & 0 & 0 & 0 & 0 & 1 & 0 \\ -0.556 & 0 & 0 & 0 & 0 & 0 & 0 & 1 \end{bmatrix},$$

$$\mathbf{b} = \begin{bmatrix} 0.909 \\ 1 \\ 0.889 \\ 1.091 \\ 1 \\ 1.111 \end{bmatrix}.$$

In this case, the number s of different sets $\mathcal{I}$ is 15:

$$\begin{array}{lllll} \{5,6\} & \{4,6\} & \{4,5\} & \{3,6\} & \{3,5\} \\ \{3,4\} & \{2,6\} & \{2,5\} & \{2,4\} & \{2,3\} \\ \{1,6\} & \{1,5\} & \{1,4\} & \{1,3\} & \{1,2\} \end{array}$$

Among these, the sets

$$\{3,6\} \quad \{2,5\} \quad \{1,4\}$$

give singular $\mathbf{B}_k$ matrices, while the sets

$$\{4,5\} \quad \{3,5\} \quad \{3,4\} \quad \{2,6\} \quad \{1,6\} \quad \{1,2\}$$

originate nonfeasible solutions (negative σ_i terms). Therefore, only 6 permutations (6 $\mathbf{B}_k$ matrices) remain, that define the vertices of the polytope P_x, and correspondingly those of P_q and P_u:

$$P_q = \left\{ \begin{bmatrix} -0.5 \\ -1 \\ -1 \end{bmatrix}, \begin{bmatrix} -1.2 \\ 0.4 \\ -1 \end{bmatrix}, \begin{bmatrix} -1.2 \\ 1 \\ -0.7 \end{bmatrix}, \begin{bmatrix} 0.3 \\ 1 \\ 0.8 \end{bmatrix}, \begin{bmatrix} 1 \\ -0.4 \\ 0.8 \end{bmatrix}, \begin{bmatrix} 1 \\ -1 \\ 0.5 \end{bmatrix} \right\},$$

$$P_x = \left\{ \begin{bmatrix} -2 \\ -2 \end{bmatrix}, \begin{bmatrix} -2 \\ 0.8 \end{bmatrix}, \begin{bmatrix} -1.4 \\ 2 \end{bmatrix}, \begin{bmatrix} 1.6 \\ 2 \end{bmatrix}, \begin{bmatrix} 1.6 \\ -0.8 \end{bmatrix}, \begin{bmatrix} 1 \\ -2 \end{bmatrix} \right\}, \tag{21}$$

$$P_u = \left\{ \begin{bmatrix} 1.5 \\ -0.5 \\ 0 \\ 0 \\ 0 \\ 0.5 \end{bmatrix}, \begin{bmatrix} 2.2 \\ -1.2 \\ 0 \\ 0 \\ 0 \\ 1.2 \end{bmatrix}, \begin{bmatrix} 1.9 \\ -1.2 \\ 0 \\ 0 \\ 0 \\ 1.2 \end{bmatrix}, \begin{bmatrix} -1.1 \\ 0.3 \\ 0 \\ 0 \\ 0 \\ -0.3 \end{bmatrix}, \begin{bmatrix} -1.8 \\ 1 \\ 0 \\ 0 \\ 0 \\ -1 \end{bmatrix}, \begin{bmatrix} -1.5 \\ 1 \\ 0 \\ 0 \\ 0 \\ -1 \end{bmatrix} \right\}.$$

The polytopes are represented in Fig. 4, where vertices are labeled in the order they are enumerated in (21). Assuming for simplicity $\mathbf{W}_u = \mathbf{I}$, the maximum output performance is obtained at vertex B.

Redundant Systems: The velocity workspace analysis for redundant systems can be carried out in an analogous way, i.e. by evaluating the vertices of a polytope in the parameter space, then searching for extremum performances among them. However, a formal justification of this procedure takes a little more geometric reasoning than in the nonredundant case.

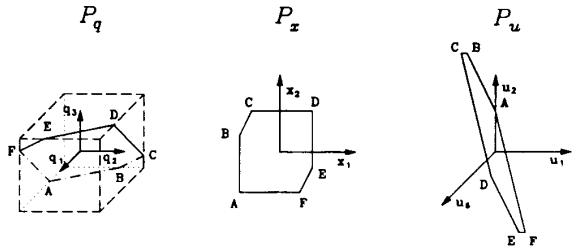

Fig. 4. The joint-space, parameter-space, and task-space polytopes for Example 2.

For redundant systems, the input space polytope P_r is the intersection of P_r' with the affine manifold $\Pi_r \stackrel{\text{def}}{=} \{\dot{\mathbf{r}} \in R^{\mathbf{r}}\colon \mathbf{DC}_{22}\mathbf{x} + \mathbf{DC}_{23}\mathbf{y} + \dot{r}_o.\mathbf{x} \in R^{N_c}.\mathbf{y} \in R^{N_r}\}$. Again, a convex polytope P_{xy} in $R^{N_c+N_r}$ is implicitly defined by $P_{xy} \stackrel{\text{def}}{=} \{\mathbf{x} \in R^{N_c}.\mathbf{y} \in R^{N_r}\colon \|\dot{\mathbf{r}}\|_\infty = \|\mathbf{DC}_{22}\mathbf{x} + \mathbf{DC}_{23}\mathbf{y} + \dot{\mathbf{r}}_o\|_\infty \leq 1\}$. Since $\mathbf{D}$ is invertible and $[\mathbf{C}_{22}\ \mathbf{C}_{23}]$ is full column rank, every vertex of P_{xy} is mapped by one and only one vertex of P_r. Unlike the nonredundant case, however, the mapping between P_{xy} and the polytope in the task space, P_u, is not a bijection for redundant manipulators. Nevertheless, maximum values of (19) are still obtained in correspondence of vertices of P_u. These vertices are the image under $\mathbf{C}_{12}$ of points on the boundary of P_{xy}. In particular, they are at least the image of the vertices of the polytope $P_x \stackrel{\text{def}}{=} \{\mathbf{x} \in R^{N_c}.\mathbf{y} = 0\colon \|\dot{\mathbf{r}}\|_\infty = \|\mathbf{DC}_{22}\mathbf{x} + \dot{\mathbf{r}}_o\|_\infty = 1\}$. In fact, recalling that:

- $\mathbf{C}_{23}\mathbf{y} \in \mathcal{N}(\mathbf{HJ}), \forall \mathbf{y} \in R^{N_r}$, i.e. only the term $\mathbf{C}_{22}\mathbf{x}$ affects the output velocity;
- if $\|\mathbf{DC}_{22}\mathbf{x} + \dot{\mathbf{r}}_o\|_\infty < 1$ then $\|\dot{\mathbf{u}}\|_2 = \sqrt{\mathbf{x}^T\mathbf{C}_{12}^T\mathbf{W}_u\mathbf{C}_{12}\mathbf{x}} < \|\dot{\mathbf{u}}\|_{2,\max}$, i.e., a maximum output performance may be obtained only in a point for which $\|\mathbf{DC}_{22}\mathbf{x} + \dot{\mathbf{r}}_o\|_\infty = 1$;

it follows that any change of the value of $\mathbf{y}$ from a vertex of P_{xy} corresponding to a maximum output performance does not affect neither $\|\dot{\mathbf{u}}\|_2$ nor $\|\dot{\mathbf{r}}\|_\infty$. Therefore, a bijection may be established between P_u and P_x.

In conclusion, the same algorithm for the computation of the vertices of the polytopes P_u, P_r and P_x utilized for the nonredundant case may be adopted, provided that the constraint equation terms are suitably modified as

$$\mathbf{A} = \begin{bmatrix} \mathbf{DC}_{22} & \mathbf{DC}_{23} \\ & \mathbf{I} \\ -\mathbf{DC}_{22} & -\mathbf{DC}_{23} \end{bmatrix}, \quad \mathbf{z} = \begin{bmatrix} \mathbf{x} \\ \mathbf{y} \\ \sigma \end{bmatrix}.$$

Then, polytope P_x is evaluated from P_{xy} by imposing $\mathbf{y} = 0$.

Example 1 (Part d): Consider again the whole-limb robot of example 2, with soft finger contacts. Assume now that $q_1 = 1.128$ [rad], $q_2 = 0$, $q_3 = \pi/2$, $u = 0.5178$, $v = 1[m]$. The first limb is now in singular configuration and, as observed in Section II-A, the system has now one degree of redundancy ($N_r = 1$). In this case, the kinematic analysis matrices are:

$$\mathbf{C}_{12} = \begin{bmatrix} -1.11 \\ .52 \\ 0 \\ 0 \\ 0 \\ -.52 \end{bmatrix}, \quad \mathbf{C}_{22} = \begin{bmatrix} .48 \\ 0 \\ .58 \end{bmatrix}, \quad \mathbf{C}_{23} = \begin{bmatrix} -.24 \\ .58 \\ 0 \end{bmatrix}.$$

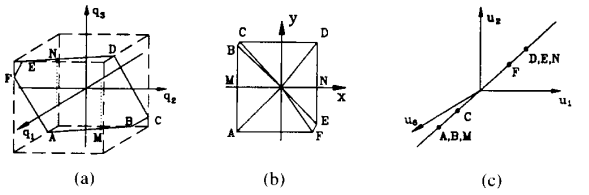

Fig. 5. The joint-space (a), parameter-space (b), and task-space (c) polytopes for Example 1(d).

The polytopes corresponding to the given bounds are:

$$P_{xy} = \left\{ \begin{bmatrix} -1.71 \\ -1.71 \end{bmatrix}, \begin{bmatrix} -1.71 \\ 1.56 \end{bmatrix}, \begin{bmatrix} -1.63 \\ 1.71 \end{bmatrix}, \begin{bmatrix} 1.37 \\ 1.71 \end{bmatrix}, \begin{bmatrix} 1.37 \\ -1.41 \end{bmatrix}, \begin{bmatrix} 1.21 \\ -1.71 \end{bmatrix} \right\},$$

$$P_q = \left\{ \begin{bmatrix} -.39 \\ -1 \\ -1 \end{bmatrix}, \begin{bmatrix} -1.2 \\ 0.91 \\ -1 \end{bmatrix}, \begin{bmatrix} -1.2 \\ 1 \\ -.95 \end{bmatrix}, \begin{bmatrix} 0.23 \\ 1 \\ 0.8 \end{bmatrix}, \begin{bmatrix} 1 \\ -.82 \\ 0.8 \end{bmatrix}, \begin{bmatrix} 1 \\ -1 \\ 0.71 \end{bmatrix} \right\},$$

$$P_u = \left\{ \begin{bmatrix} 1.9 \\ -.9 \\ 0 \\ 0 \\ 0 \\ 0.9 \end{bmatrix}, \begin{bmatrix} 1.9 \\ -.9 \\ 0 \\ 0 \\ 0 \\ 0.9 \end{bmatrix}, \begin{bmatrix} 1.81 \\ -0.86 \\ 0 \\ 0 \\ 0 \\ 0.86 \end{bmatrix}, \begin{bmatrix} -1.52 \\ 0.72 \\ 0 \\ 0 \\ 0 \\ -0.72 \end{bmatrix}, \begin{bmatrix} -1.52 \\ 0.72 \\ 0 \\ 0 \\ 0 \\ -0.72 \end{bmatrix}, \begin{bmatrix} -1.34 \\ 0.64 \\ 0 \\ 0 \\ 0 \\ -0.64 \end{bmatrix} \right\}.$$

The polytopes are shown in Fig. 5, and vertices are labeled in the order they are enumerated. Note that in this case there is only one possible motion for the object ($N_c = 1$), and in fact the vertices of polytope P_u lie along a line in the twist space. Assuming for simplicity $\mathbf{W}_u = \mathbf{I}$, the maximum performance corresponds to vertex A (or B). Note that polytope P_u is the mapping in task velocity space of P_x

$$P_x = \{[-1.71], [-1.71], [-1.63], [1.37], [1.37], [1.21]\}$$
$$= \{[-1.71], [-1.63]. [1.37], [1.21]\},$$

In Fig. 5, polytopes P_u, P_{xy}, P_q, and P_x are shown. Points M and N in Fig. 5(a) and Fig. 5(b) are the two vertices of P_x, which are mapped in points $A \equiv B$ and $D \equiv E$ of P_u.

V. Case Studies

A. Case Study 1

As a first application of the manipulability analysis methods above described, consider the system depicted in Fig. 6, consisting of two two-link limbs rigidly grasping an object.

By applying the technique of Section II, we obtain

$$\mathbf{C}_{12} = \begin{bmatrix} Ll_1l_2 \sin q_1 \sin q_3 \\ -Ll_1l_2 \cos q_1 \sin q_3 \\ 0 \\ 0 \\ 0 \\ l_1l_2 \sin(q_3 - q_1) \end{bmatrix};$$

$$\mathbf{C}_{22} = \begin{bmatrix} l_1l_2 \sin(q_3 - q_1) - Ll_2 \sin q_3 \\ Ll_2 \sin q_3 \\ l_1l_2 \sin(q_3 - q_1) - Ll_1 \sin q_1 \\ Ll_1 \sin q_1 \end{bmatrix}.$$

Correspondingly, the manipulability ellipsoid degenerates in a segment. In this case the performance-to-effort ratio, assuming $\mathbf{W}_u = \text{diag}[1, 1, 1, L, L, L]$, evaluates to the equation shown at the bottom of this page. Other proposed generalizations of the manipulability ellipsoid method fail when applied to general (including kinematically defective) cooperating robot systems. In Fig. 7(a) and Fig. 7(b) are reported the ellipsoids as evaluated by the methods proposed in [23] and [24], respectively, for the particular configuration $q_1 = q_3 = \pi/2$ depicted in Fig. 6(b). Note that both methods result in ellipsoids with a nonnull minor axis, indicating a possibility of motion of the object in the y direction, which is clearly negated by the system (actually, a four-bar linkage). The ellipsoid resulting from the method proposed in this paper, in the configuration of Fig. 6(b), is reported in Fig. 7(c).

In this case, also the velocity polytopes degenerate to a segment. Assuming $l_1 = l_2 = 1, L = 2[m]$, and $q_{i,\min} = -1, q_{i,\max} = 1[\text{rad}/s]$, the algorithm presented in Section IV gives:

$$P_x = \{[-0.5], [0.5], \}. \quad P_q = \left\{ \begin{bmatrix} 1 \\ -1 \\ -1 \\ 1 \end{bmatrix}, \begin{bmatrix} -1 \\ 1 \\ 1 \\ -1 \end{bmatrix} \right\}$$

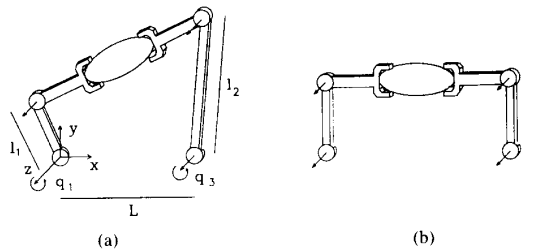

(a) (b)

Fig. 6. Manipulation system of case study 1: (a) generic configuration; (b) particular configuration considered in text.

$$P_u = \left\{ \begin{bmatrix} 1 \\ 0 \\ 0 \\ 0 \\ 0 \\ 0 \end{bmatrix}, \begin{bmatrix} -1 \\ 0 \\ 0 \\ 0 \\ 0 \\ 0 \end{bmatrix} \right\}. \tag{22}$$

In this degenerate case, both the polytope and the ellipsoid methods give substantially the same result (i.e. a segment).

B. Case Study 2

In this example, we will consider two four-degrees of freedom, SCARA-type robots manipulating an object, as shown in Fig. 8. For simplicity, all the links of the two robots are assumed to have the same length L. If two complete-constraint contacts are used to model the grip on the object, we obtain the matrices shown at the bottom of this page. Note that, for nonsingular configurations ($q_2 \neq 0$, $q_6 \neq 0$), the system has connectivity $N_c = 3$, no redundancy nor indeterminacy, and $\mathbf{C}_{12} = \mathbf{C}_1$, $\mathbf{C}_{22} = \mathbf{C}_2$. Feasible first-order differential motions for the object are all pure translations (the last three rows of $\mathbf{C}_{12}$ are zeroes), achieved by moving the joints with suitable combinations of the columns of $\mathbf{C}_{22}$.

$$R_c^2 = \frac{1}{2} \times \frac{L^2 l_1^2 l_2^2 \left(\sin^2 q_1 + \sin^2(q_3 - q_1) \right)}{l_1^2 l_2^2 \sin^2(q_3 - q_1) + L^2(l_1^2 \sin^2 q_1 + l_2^2 \sin^2 q_3) - Ll_1l_2(l_1 \sin q_1 + l_2 \sin q_3) \sin(q_3 - q_1)}$$

$$\mathbf{C}_1 = \begin{bmatrix} L \sin q_2 & 0 & 0 \\ 0 & L \sin q_2 \sin q_6 & 0 \\ 0 & 0 & L \sin q_6 \\ 0 & 0 & 0 \\ 0 & 0 & 0 \\ 0 & 0 & 0 \end{bmatrix}.$$

$$\mathbf{C}_2 = \begin{bmatrix} \cos(q_1 + q_2) & \sin(q_1 + q_2) \sin q_6 & 0 \\ -\cos q_1 - \cos(q_1 + q_2) & -(\sin q_1 + \sin(q_1 + q_2)) \sin q_6 & 0 \\ \cos q_1 & \sin q_1 \sin q_6 & 0 \\ 0 & 0 & L \sin q_6 \\ 0 & \cos(q_5 + q_6) \sin q_2 & \sin(q_5 + q_6) \\ 0 & -(\cos q_5 + \cos(q_5 + q_6)) \sin q_2 & -\sin q_5 - \sin(q_5 + q_6) \\ 0 & \cos q_5 \cos q_2 & \sin q_5 \\ L \sin q_2 & 0 & 0 \end{bmatrix}$$

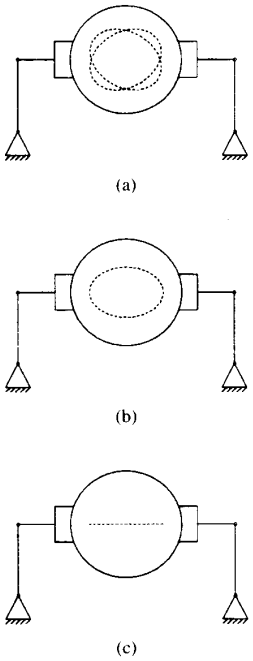

Fig. 7. Manipulability ellipsoids for the system of case study 1 in configuration in Fig. 6(b), according to three different methods: (a) Method described in [23]; (b) Method described in [24]; (c) Method proposed in this paper.

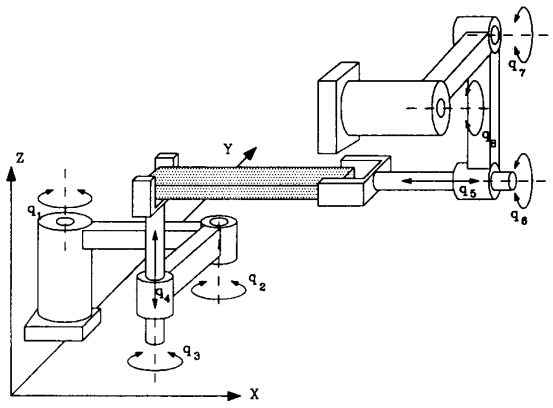

Fig. 8. Two 4-axis SCARA robots cooperating to manipulate an object.

If either arm is in singular configuration, $\mathbf{C}_1$ looses rank, hence connectivity is lost to the advantage of redundancy. Thus, for $q_2 = 0$, the block decomposition is

$$\mathbf{C}_{12} = \begin{bmatrix} 0 \\ 0 \\ L\sin q_6 \\ 0 \\ 0 \\ 0 \end{bmatrix}, \quad \mathbf{C}_{22} = \begin{bmatrix} 0 \\ 0 \\ 0 \\ L\sin q_6 \\ \sin(q_5+q_6) \\ -\sin q_5 - \sin(q_5+q_6) \\ \sin q_5 \\ 0 \end{bmatrix};$$

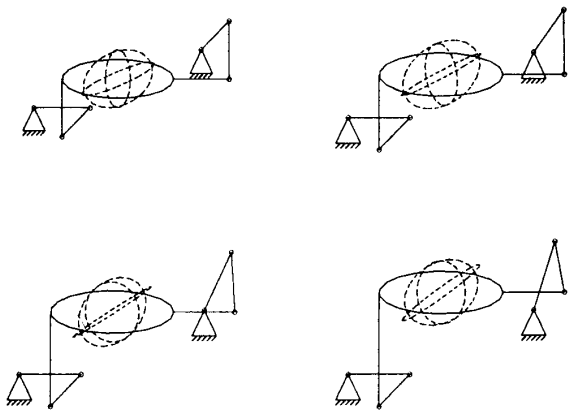

Fig. 9. Manipulability ellipsoids in four different configurations of the system of case study 2. The object is being lifted in the vertical direction. Axonometric views of the three principal ellipses in the translational task space are used for display.

$$\mathbf{C}_{23} = \begin{bmatrix} 1 \\ -2 \\ 1 \\ 0 \\ 0 \\ 0 \\ 0 \\ 0 \end{bmatrix}.$$

Note that the decomposition above shows that the mobility of the system is not preserved in singular configurations. Finally, if both arms are in singular configuration ($q_2 = q_6 = 0$), no first-order differential motion of the object is possible, while two redundant degrees of freedom are present:

$$\mathbf{C}_{23} = \begin{bmatrix} 1 & 0 \\ -2 & 0 \\ 1 & 0 \\ 0 & 0 \\ 0 & 1 \\ 0 & -2 \\ 0 & 1 \\ 0 & 0 \end{bmatrix}.$$

The manipulability ellipsoids in four different configurations of the system during the vertical lift of the object are reported in Fig. 9.

The velocity polytopes, in the configuration shown in Fig. 8, with $q_1 = q_5 = q_2 = q_6 = q_3 = q_7 = \pi/2, q_4 = q_8 = 1\ [m]$, evaluate to

$$P_x = \left\{ \begin{bmatrix} -3.75 \\ 1 \\ -3.79 \end{bmatrix}, \begin{bmatrix} -3.75 \\ -3 \\ -3.79 \end{bmatrix}, \begin{bmatrix} 1 \\ 4 \\ -3.79 \end{bmatrix}, \begin{bmatrix} 1 \\ -4 \\ -3.79 \end{bmatrix}, \begin{bmatrix} -4.75 \\ 1 \\ 0 \end{bmatrix}, \begin{bmatrix} -4.75 \\ -3 \\ 0 \end{bmatrix}, \begin{bmatrix} -1 \\ -4 \\ 3.79 \end{bmatrix}, \begin{bmatrix} -1 \\ 4 \\ 3.79 \end{bmatrix}, \begin{bmatrix} 4.75 \\ -1 \\ 0 \end{bmatrix}, \begin{bmatrix} 3.75 \\ -1 \\ 3.79 \end{bmatrix}, \begin{bmatrix} 4.75 \\ 3 \\ 0 \end{bmatrix}, \begin{bmatrix} 3.75 \\ 3 \\ 3.79 \end{bmatrix} \right\},$$

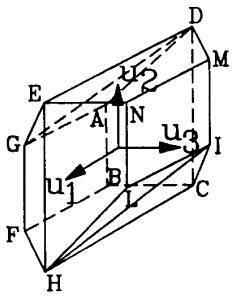

Fig. 10. Velocity polytope P_u for the cooperating SCARA robots.

$$P_q = \left\{ \begin{bmatrix} -1 \\ 0 \\ 1 \\ 0 \\ -1 \\ 1 \\ -1 \\ 0 \end{bmatrix}, \begin{bmatrix} -1 \\ 0 \\ 1 \\ -1 \\ -1 \\ 1 \\ 0 \\ -1 \end{bmatrix}, \begin{bmatrix} 0 \\ -1 \\ 1 \\ 1 \\ -1 \\ 0 \\ -1 \\ 1 \end{bmatrix}, \begin{bmatrix} 0 \\ -1 \\ 1 \\ -1 \\ -1 \\ 0 \\ 1 \\ -1 \end{bmatrix}, \begin{bmatrix} -1 \\ 1 \\ 0 \\ 0 \\ 0 \\ 1 \\ -1 \\ 0 \end{bmatrix}, \begin{bmatrix} -1 \\ 1 \\ 0 \\ -1 \\ 0 \\ 1 \\ 0 \\ -1 \end{bmatrix}, \right.$$
$$\left. \begin{bmatrix} 0 \\ 1 \\ -1 \\ -1 \\ 1 \\ 0 \\ 1 \\ -1 \end{bmatrix}, \begin{bmatrix} 0 \\ 1 \\ -1 \\ 1 \\ 1 \\ 0 \\ -1 \\ 1 \end{bmatrix}, \begin{bmatrix} 1 \\ -1 \\ 0 \\ 0 \\ 0 \\ -1 \\ 1 \\ 0 \end{bmatrix}, \begin{bmatrix} 1 \\ 0 \\ -1 \\ 0 \\ 1 \\ -1 \\ 1 \\ 0 \end{bmatrix}, \begin{bmatrix} 1 \\ -1 \\ 0 \\ 1 \\ 0 \\ -1 \\ 0 \\ 1 \end{bmatrix}, \begin{bmatrix} 1 \\ 0 \\ -1 \\ 1 \\ 1 \\ -1 \\ 0 \\ 1 \end{bmatrix} \right\}.$$

$$P_u = \left\{ \begin{bmatrix} -1 \\ -1 \\ 0 \\ 0 \\ 0 \\ 0 \end{bmatrix}, \begin{bmatrix} -1 \\ -1 \\ 0 \\ 0 \\ 0 \\ 0 \end{bmatrix}, \begin{bmatrix} -1 \\ 0 \\ -1 \\ 0 \\ 0 \\ 0 \end{bmatrix}, \begin{bmatrix} -1 \\ 0 \\ 1 \\ 0 \\ 0 \\ 0 \end{bmatrix}, \begin{bmatrix} 1 \\ 0 \\ 1 \\ 0 \\ 0 \\ 0 \end{bmatrix}, \begin{bmatrix} 0 \\ -1 \\ -1 \\ 0 \\ 0 \\ 0 \end{bmatrix}, \right.$$
$$\left. \begin{bmatrix} 0 \\ -1 \\ 0 \\ 0 \\ 0 \\ 0 \end{bmatrix}, \begin{bmatrix} 1 \\ 0 \\ -1 \\ 0 \\ 0 \\ 0 \end{bmatrix}, \begin{bmatrix} 0 \\ 1 \\ 0 \\ 0 \\ 0 \\ 0 \end{bmatrix}, \begin{bmatrix} 1 \\ 1 \\ 0 \\ 0 \\ 0 \\ 0 \end{bmatrix}, \begin{bmatrix} 0 \\ 1 \\ 1 \\ 0 \\ 0 \\ 0 \end{bmatrix}, \begin{bmatrix} 1 \\ 1 \\ 1 \\ 0 \\ 0 \\ 0 \end{bmatrix} \right\}.$$

In this case, the bounds on joint velocities are assumed unitary, i.e. $q_{i,\min} = -1$; $q_{i,\max} = 1$. The velocity polytope P_u is shown in Fig. 10.

C. Case Study 3

A more complex manipulator will be considered as a final example. The MIT Whole-Arm Manipulator ("WAM") [10], depicted in Fig. 11, is comprised of three links, of which one is fixed (base, or chest, and shoulder) and two form the manipulator arm. The manipulator possesses 4 degrees of freedom: a spherical joint at the base of the first arm link, and a rotational joint between the first and the second arm links. Consider the particular configuration shown in Fig. 11. The origin of the first three reference frames are placed at the shoulder center, $\mathbf{o}_1 = \mathbf{o}_2 = \mathbf{o}_3 = [0\ 0\ 0.5]^T$ $[m]$. Also, for the configuration being considered, assume

$$\mathbf{o}_4 = [0 \quad .5 \quad 1]^T \ [m];$$
$$\mathbf{z}_1 = [1 \quad 0 \quad 0]^T; \qquad \mathbf{z}_2 = [0 \quad 0 \quad 1]^T;$$
$$\mathbf{z}_3 = [0 \quad \tfrac{\sqrt{2}}{2} \quad \tfrac{\sqrt{2}}{2}]^T; \qquad \mathbf{z}_4 = [-1 \quad 0 \quad 0]^T.$$

The arm holds an object against the base (or chest), as shown in Fig. 11, being the two contact points and their respective unit normal vectors given by

$$\mathbf{c}_1 = [0 \quad 0.6 \quad 0.8]^T m; \qquad \mathbf{c}_2 = [0 \quad 0.5 \quad 0]^T m;$$
$$\mathbf{n}_1 = \left[0 \quad -\tfrac{\sqrt{2}}{2} \quad -\tfrac{\sqrt{2}}{2}\right]^T; \qquad \mathbf{n}_2 = [0 \quad 0 \quad 1]^T.$$

Assuming soft-finger contacts, the $\mathbf{HJ}$ and $\mathbf{HG}^T$ matrices for the given configuration are computed as

$$\mathbf{J}^T\mathbf{H}^T = \begin{bmatrix} 0 & -0.3 & 0.6 & 0 & 0 & 0 & 0 & 0 \\ -0.6 & 0 & 0 & 0 & 0 & 0 & -0.71 & 0 \\ -0.21 & 0 & 0 & 0 & 0 & 0 & -1 & 0 \\ 0 & -0.2 & -0.1 & 0 & 0 & 0 & 0 & 0 \end{bmatrix};$$

$$\mathbf{GH}^T = \begin{bmatrix} 1 & 0 & 0 & 1 & 0 & 0 & 0 & 0 \\ 0 & 1 & 0 & 0 & 1 & 0 & 0 & 0 \\ 0 & 0 & 1 & 0 & 0 & 1 & 0 & 0 \\ 0 & -0.8 & 0.6 & 0 & 0 & 0.5 & 0 & 0 \\ 0.8 & 0 & 0 & 0 & 0 & 0 & -0.71 & 0 \\ -0.6 & 0 & 0 & -0.5 & 0 & 0 & -0.71 & 1 \end{bmatrix},$$

respectively. Block matrices describing the system kinematics, expressed with respect to a frame located at the center of the object, are obtained as

$$\mathbf{C}_{12} = \begin{bmatrix} 0 & 0.039 \\ 0.019 & 0 \\ -0.002 & 0 \\ -0.047 & 0 \\ 0 & 0.097 \\ 0 & 0 \end{bmatrix} \qquad \mathbf{C}_{22} = \begin{bmatrix} -0.031 & 0 \\ 0 & -0.205 \\ 0 & 0.214 \\ -0.14 & 0 \end{bmatrix}.$$

Connectivity is $N_c = 2$, while no redundancy nor indeterminacy are present. The manipulability ellipsoid degenerates in an ellipse with principal axes

$$A_1 = \begin{bmatrix} 0.36 \\ 0 \\ 0 \\ 0 \\ 0.45 \\ 0 \end{bmatrix}, \qquad A_2 = \begin{bmatrix} 0 \\ -0.27 \\ 0.2 \\ 0.33 \\ 0 \\ 0 \end{bmatrix}.$$

Assuming unitary bounds on the joint limits, the velocity polytopes result

$$P_x = \left\{ \begin{bmatrix} 7.13 \\ -4.68 \end{bmatrix}, \begin{bmatrix} -7.13 \\ -4.68 \end{bmatrix}, \begin{bmatrix} 7.13 \\ 4.68 \end{bmatrix}, \begin{bmatrix} -7.13 \\ 4.68 \end{bmatrix} \right\},$$

$$P_q = \left\{ \begin{bmatrix} -0.22 \\ 0.96 \\ -1 \\ -1 \end{bmatrix}, \begin{bmatrix} 0.22 \\ 0.96 \\ -1 \\ 1 \end{bmatrix}, \begin{bmatrix} -0.22 \\ -0.96 \\ 1 \\ -1 \end{bmatrix}, \begin{bmatrix} 0.22 \\ -0.96 \\ 1 \\ 1 \end{bmatrix} \right\},$$

$$P_u = \left\{ \begin{bmatrix} -0.18 \\ 0.13 \\ -0.017 \\ -0.33 \\ -0.45 \\ 0 \end{bmatrix}, \begin{bmatrix} -0.18 \\ -0.13 \\ 0.017 \\ 0.33 \\ -0.45 \\ 0 \end{bmatrix}, \begin{bmatrix} 0.18 \\ 0.13 \\ -0.017 \\ -0.33 \\ 0.45 \\ 0 \end{bmatrix}, \begin{bmatrix} 0.18 \\ -0.13 \\ 0.017 \\ 0.33 \\ 0.45 \\ 0 \end{bmatrix} \right\}.$$

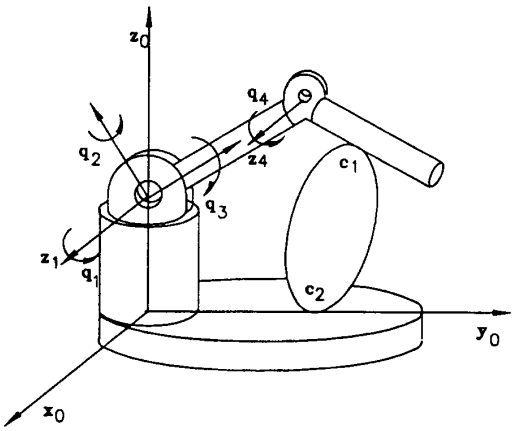

Fig. 11. MIT-AI Lab whole-arm manipulator (WAM) rolling an object on its base.

VI. Conclusion

In this paper, we considered multiple robot systems for coordinated manipulation of objects. With respect to prior results, the more general case when kinematically defective elements are present in the system has been explicitly addressed. Such widening of the analysis scope is believed to be both theoretically interesting and practically important, since it allows to consider cooperating systems comprised of several simple (few joints) linkages, whole-limb manipulators, devices for power-grasping, parallel manipulators, etc.

The contributions of this paper are in the definition of algorithms for analyzing the mobility and differential kinematics of such systems, and in extending the concepts of manipulability ellipsoids and polytopes previously proposed for simpler systems.

Future work in this area will address the extension to force/torque and dynamic manipulability ellipsoids. Also, the possible usefulness and significance of using different norms (p-norms or others) for the evaluation of joint and task space performances, that led in this paper to a convenient reformulation of the polytope method for velocity workspace analysis, will be further investigated.

Appendix A
Definitions and Notation

The quantities used in writing the differential kinematics of cooperating limbs are defined as follows:

$$
{}^{o}\dot{\mathbf{x}} = \left[{}^{o}\dot{\mathbf{c}}_1^T, \ldots, {}^{o}\dot{\mathbf{c}}_n^T, {}^{o}\omega_1^T, \ldots, {}^{o}\omega_n^T\right]^T; \quad {}^{o}\dot{\mathbf{x}} \in R^{6n};
$$

$$
{}^{m}\dot{\mathbf{x}} = \left[{}^{m}\dot{\mathbf{c}}_1^T, \ldots, {}^{m}\dot{\mathbf{c}}_n^T, {}^{m}\omega_1^T, \ldots, {}^{m}\omega_n^T\right]^T; \quad {}^{m}\dot{\mathbf{x}} \in R^{6n};
$$

$$
\dot{\mathbf{u}} = [\mathbf{v}^T, \omega^T]^T; \quad \dot{\mathbf{u}} \in R^6;
$$

$$
\dot{\mathbf{q}} = [\dot{q}_1, \dot{q}_2, \ldots, \dot{q}_r]^T; \quad \dot{\mathbf{q}} \in R^r;
$$

$$
\mathbf{G} = \begin{bmatrix} \mathbf{I}_3 & \cdots & \mathbf{I}_3 & \mathbf{O}_{3\times 3n} & \\ \mathbf{c_1}\times & \cdots & \mathbf{c_n}\times & \mathbf{I}_3 & \cdots & \mathbf{I}_3 \end{bmatrix}; \quad \mathbf{G} \in R^{6\times 6n}
$$

$$
\mathbf{J}^T = \begin{bmatrix} \mathbf{D}_{1,1} & \cdots & \mathbf{D}_{n,1} & \mathbf{L}_{1,1} & \cdots & \mathbf{L}_{n,1} \\ \cdots & \cdots & \cdots & \cdots & \cdots & \cdots \\ \mathbf{D}_{1,r} & \cdots & \mathbf{D}_{n,r} & \mathbf{L}_{1,r} & \cdots & \mathbf{L}_{n,r} \end{bmatrix}; \quad \mathbf{J} \in R^{6n\times r};
$$

where $\mathbf{c_i}\times$ is the cross-product matrix for $\mathbf{c}_i$ (i.e. the skew-symmetric matrix such that $\mathbf{c_i}\times\omega = \mathbf{c}_i \times \omega$); blocks $\mathbf{D}_{i,j}$ and $\mathbf{L}_{i,j}$ are defined as

$$
\mathbf{D}_{i,j} = \begin{cases} [0 \quad 0 \quad 0] & \text{if the } i\text{-th contact force does not affect the } j\text{-th joint;} \\ \mathbf{z}_j^T & \text{for prismatic } j\text{-th joint;} \\ \mathbf{z}_j^T(\mathbf{c_i} - \mathbf{o_j}\times) & \text{for rotational } i\text{-th joint;} \end{cases}
$$

$$
\mathbf{L}_{i,j} = \begin{cases} (0 \quad 0 \quad 0) & \text{if the } i\text{-th contact force does not affect the } j\text{-th joint;} \\ (0 \quad 0 \quad 0) & \text{for prismatic } j\text{-th joint;} \\ \mathbf{z}_j^T & \text{for rotational } j\text{-th joint;} \end{cases};
$$

and $\mathbf{o}_j$ and $\mathbf{z}_j$ are the center and z-axis unit vector of the Denavit-Hartenberg frames associated with the jth joint.

The selection matrix is built as follows. Assume the variables relative to complete-constraint contacts are numbered from 1 to n_1, those relative to soft-finger contacts from n_1+1 to n_1+n_2, and those relative to hard-finger contacts from n_1+n_2+1 to $n_1+n_2+n_3=n$. The $\mathbf{H}$ matrix is written as

$$
\mathbf{H} = \begin{bmatrix} \mathbf{I}_{3(n+n_1)} & & \mathbf{O}_{3(n+n_1)\times 3(n_2+n_3)} & & \\ & \mathbf{n}_{n_1+1}^T & \cdots & 0\ 0\ 0 & \\ \mathbf{O}_{n_2\times 3(n+n_1)} & \cdots & \cdots & \cdots & \mathbf{O}_{n_2\times 3n_3} \\ & 0\ 0\ 0 & \cdots & \mathbf{n}_{n_1+n_2}^T & \end{bmatrix},
$$

where $\mathbf{n}_i$ is the unit vector normal to the surfaces at the ith contact point $\mathbf{c}_i$.

Appendix B
Algorithm for Obtaining $\mathbf{C}$ in (6)

Recall that any $p \times q$ matrix $\mathbf{A}$ whose rank is ρ can be decomposed (by Gaussian elimination) in a row-reduced echelon form (RREF) as

$$
\mathbf{PA} = \mathbf{L}\begin{bmatrix}\mathbf{U} \\ \mathbf{O}\end{bmatrix},
$$

where $\mathbf{P}$ is a $p \times p$ permutation matrix, $\mathbf{L}$ is $p \times p$ lower-triangular invertible, $\mathbf{U}$ is $\rho \times q$ "staircase", and the zero block is $(p-\rho)\times q$.

By reordering columns of $\mathbf{A}$ one can further obtain

$$
\mathbf{PAP}' = \mathbf{L}\begin{bmatrix}\mathbf{U}_1 & \mathbf{U}_2 \\ \mathbf{O} & \mathbf{O}\end{bmatrix},
$$

where $\mathbf{P}'$ is a $q \times q$ permutation matrix, $\mathbf{U}_1$ is $\rho \times \rho$ upper triangular invertible, $\mathbf{U}_2$ is $\rho \times (q-\rho)$, and the zero blocks have suitable dimensions.

The latter decomposition can be used to obtain a matrix $\mathbf{N}_A$ whose columns span the nullspace of $\mathbf{A}$,

$$
\mathbf{N}_A = \mathbf{P}'\begin{bmatrix}\mathbf{U}_1^{-1}\mathbf{U}_2 \\ \\ -\mathbf{I}_{q-\rho}\end{bmatrix}.
$$

Note that the columns of $\mathbf{U}_1^{-1}\mathbf{U}_2$ can be evaluated simply by back substitution in the $q-\rho$ triangular systems $\mathbf{U}_1\mathbf{x} = \mathbf{U}_2$. Linearly dependent columns may possibly enter $\mathbf{N}_A$, and must be purged to obtain a minimal basis of $\mathcal{N}(\mathbf{A})$. Note that this algorithm, although not numerically optimal, can be easily implemented also in symbolic form.

The RREF algorithm (in its first form) can be employed to reduce the kinematic basis matrix $\mathbf{C} = [\mathbf{C}_1^T \quad \mathbf{C}_2^T]^T$ to its block form (6), by operating as follows ($\mathbf{R} \rightarrow \mathbf{X}$ means "assign result $\mathbf{R}$ to variable $\mathbf{X}$"):

Step 1 Apply RREF to $\mathbf{C}_1^T$ and transpose the result, to obtain

$$\mathbf{C}_1\mathbf{P}_1^T\mathbf{L}_1^{-T} = [\mathbf{U}_{C_1} \quad \mathbf{O}] \rightarrow \mathbf{C}_1;$$

where the zero block has N_r columns;

Step 2 Apply the same column operations on $\mathbf{C}_2$

$$\mathbf{C}_2\mathbf{P}_1^T\mathbf{L}_1^{-T} \rightarrow \mathbf{C}_2;$$

Step 3 Apply RREF to the first $m - N_r$ rows of $\mathbf{C}_2^T$ and transpose, thus obtaining N_l null columns on the right; apply the same operations on the first $m - N_r$ columns of $\mathbf{C}_1$; at his point, matrix $\mathbf{C}$ has the following structure:

$$\begin{bmatrix} \mathbf{C}_{12} & \mathbf{C}_{11} & \mathbf{O} \\ \mathbf{C}_{22} & \mathbf{O} & \mathbf{C}_{23} \end{bmatrix}$$

Step 4 Reassemble matrix $\mathbf{C}$ by permuting the first and second block of columns: (6) is obtained.

APPENDIX C
EXAMPLE 1

With reference to Fig. 1, the contact point coordinates $\mathbf{c}_1, \mathbf{c}_2$ and normal unit vectors $\mathbf{n}_1, \mathbf{n}_2$ are

$$\mathbf{c}_1 = \begin{bmatrix} l_1\cos q_1 + u\cos(q_1+q_2) \\ l_1\sin q_1 + u\sin(q_1+q_2) \\ 0 \end{bmatrix}, \quad \mathbf{c}_2 = \begin{bmatrix} L + v\cos q_3 \\ v\sin q_3 \\ 0 \end{bmatrix},$$

$$\mathbf{n}_1 = \begin{bmatrix} \sin(q_1+q_2) \\ -\cos(q_1+q_2) \\ 0 \end{bmatrix}, \quad \mathbf{n}_2 = \begin{bmatrix} -\sin q_3 \\ \cos q_3 \\ 0 \end{bmatrix}.$$

All joints have axis parallel to the z axis, and centers in

$$\mathbf{o}_1 = \begin{bmatrix} 0 \\ 0 \\ 0 \end{bmatrix}, \quad \mathbf{o}_2 = \begin{bmatrix} l_1\cos q_1 \\ l_1\sin q_1 \\ 0 \end{bmatrix},$$

$$\mathbf{o}_3 = \begin{bmatrix} L \\ 0 \\ 0 \end{bmatrix}, \quad \mathbf{o}_4 = \begin{bmatrix} L + l_2\cos q_3 \\ l_2\sin q_3 \\ 0 \end{bmatrix}.$$

If both contacts are hard-finger, $\mathbf{H} = [\mathbf{I}_6 \mid \mathbf{O}_{6\times 6}]$; if both contacts are complete-constraint, $\mathbf{H} = \mathbf{I}_{12}$; finally, if both contacts are soft-finger,

$$\mathbf{H} = \begin{bmatrix} \mathbf{I}_6 & \mathbf{O}_{6\times 6} \\ \mathbf{O}_{2\times 6} & \begin{matrix} \mathbf{n}_1^T & 0\,0\,0 \\ 0\,0\,0 & \mathbf{n}_2^T \end{matrix} \end{bmatrix};$$

In the latter case, the $\mathbf{Q}$ matrix of (5) is given by the equation shown at the bottom of this page, where standard abbreviations $S_{ij} = \sin(q_i + q_j)$, $C_{ij} = \cos(q_i + q_j)$, are used. Numerical examples have been worked out assuming the following dimensions: $l_1 = \sqrt{2}/2$, $l_2 = \sqrt{2}$, $L = 1$. The object is a sphere of radius 0.25.

A. Contact Kinematics

In deriving the equations of motion for Example 1, we adopt the description of differential kinematics of rolling contacts as presented by [31]. For the spherical object rolling on the planar surface of the i-th link, the equations governing the evolution of the local coordinates of the contact point on the object (u_{oi}, v_{oi}) and on the link (u_{fi}, v_{fi}) are

$$\begin{aligned} \dot{u}_{oi} &= \omega_{ti1}/\cos v_{oi} \\ \dot{v}_{oi} &= \omega_{ti2} \\ \dot{u}_{fi} &= \rho\omega_{ti1}\ \cos\psi_i - \rho\omega_{ti2}\ \sin\psi_i. \\ \dot{v}_{fi} &= -\rho\omega_{ti1}\ \sin\psi_i - \rho\omega_{ti2}\cos\psi_i \\ \dot{\psi}_i &= \omega_{ti1}\ \tan v_{oi} \end{aligned} \tag{23}$$

where ρ is the radius of the sphere, and ω_{ti} is the relative rotational velocity projected onto the tangent plane at the ith contact:

$$\begin{aligned} \omega_{ti} = &\begin{bmatrix} -\cos u_{oi}\sin v_{oi} & -\sin u_{oi}\sin v_{oi} & \cos v_{oi} \\ \sin u_{oi} & -\cos u_{oi} & 0 \end{bmatrix} \\ &\times R_b({}^b\omega_{fi} - {}^b\omega_o). \end{aligned} \tag{24}$$

The rotational velocity of the i-th link and of the object expressed in base frame, ${}^b\omega_{fi}$ and ${}^b\omega_o$, respectively, are easily written in terms of joint and object velocities as

$${}^b\omega_{f1} = \begin{bmatrix} 0 & 0 & 0 \\ 0 & 0 & 0 \\ 1 & 1 & 0 \end{bmatrix} \begin{bmatrix} \dot{q}_1 \\ \dot{q}_2 \\ \dot{q}_3 \end{bmatrix},$$

$${}^b\omega_{f2} = \begin{bmatrix} 0 & 0 & 0 \\ 0 & 0 & 0 \\ 0 & 0 & 1 \end{bmatrix} \begin{bmatrix} \dot{q}_1 \\ \dot{q}_2 \\ \dot{q}_3 \end{bmatrix}, \quad {}^b\omega_o = [\mathbf{O}_{3\times 3} \quad \mathbf{I}_3]\dot{\mathbf{u}} \tag{25}$$

Joining (23), (24), and (25) we obtain the differential kinematics equation for the i-th contact coordinates $\eta_i = (u_{oi}\ v_{oi}\ u_{fi}\ v_{fi}\ \psi_i)^T$ as a function of the object and joint

$$\mathbf{Q} = \left[\mathbf{H}\mathbf{G}^T \mid -\mathbf{H}\mathbf{J}\right] =$$

$$\begin{bmatrix} 1 & 0 & 0 & 0 & 0 & -l_1S_1 + uS_{12} & -l_1S_1 + uS_{12} & -l_1S_1 + uS_{12} + l_1S_1 & 0 & 0 \\ 0 & 1 & 0 & 0 & 0 & l_1C_1 + uC_{12} & l_1C_1 + uC_{12} & l_1C_1 + uC_{12} - l_1C_1 & 0 & 0 \\ 0 & 0 & 1 & l_1S_1 + uS_{12} & -l_1C_1 + uC_{12} & 0 & 0 & 0 & 0 & 0 \\ 1 & 0 & 0 & 0 & 0 & -vS_3 & 0 & 0 & -vS_3 & 0 \\ 0 & 1 & 0 & 0 & 0 & L + vC_3 & 0 & 0 & L + vC_3 - L & 0 \\ 0 & 0 & 1 & vS_3 & -L + vC_3 & 0 & 0 & 0 & 0 & 0 \\ 0 & 0 & 0 & S_{12} & -C_{12} & 0 & 0 & 0 & 0 & 0 \\ 0 & 0 & 0 & -S_3 & C_3 & 0 & 0 & 0 & 0 & 0 \end{bmatrix},$$

velocities,

$$\begin{bmatrix} \dot{\eta}_1 \\ \dot{\eta}_2 \\ \dot{\mathbf{x}} \\ \dot{\Phi} \\ \dot{\mathbf{q}} \end{bmatrix} = A(\eta_1, \eta_2, \mathbf{x}, \Phi, q) \begin{pmatrix} \dot{\mathbf{u}} \\ \dot{\mathbf{q}} \end{pmatrix} \quad i = 1, 2. \tag{26}$$

where $\mathbf{x}$ is the position of the center of the sphere in base frame, and Φ is a set of angles describing the object orientation.

REFERENCES

[1] E. Nakano, S. Ozaki, T. Ishida, and I. Kato, "Cooperational control of the anthropomorphous manipulator 'MELARM'," in *Proc. 4th Int. Symp. Industrial Robots*, 1974.

[2] M. Uchiyama and P. Dauchez, "A symmetric hybrid position force control scheme for the coordination of two robots," in *Proc. IEEE Int. Conf. Robotics and Automat.*, 1988.

[3] I. D. Walker, R. A. Freeman, and S. I. Marcus, "Analysis of motion and internal loading of objects grasped by multiple cooperating manipulators," *Int. J. Robot. Res.*, vol. 10, no. 4, Aug. 1991.

[4] J. K. Salisbury and B. Roth, "Kinematic and force analysis of articulated mechanical hands," *ASME J. Mech. Design*, vol. 82-DET-13, 1982.

[5] J. Kerr and B. Roth, "Analysis of multifingered hands," *Int. J. Robot. Res.*, vol. 4, no. 4, 1986.

[6] Z. Li, P. Hsu, and S. S. Sastry, "Grasping and coordinated manipulation by a multifingered robot hand," *Int. J. Robot. Res.*, vol. 8, no. 4, 1989.

[7] D. E. Orin and S. Y. Oh, "Control of force distribution in robotic mechanisms containing closed kinematic chains," *J. Dyn. Sist. Meas. Cont.*, vol. 102, 1981.

[8] K. J. Waldron, "Force and motion management in legged locomotion," *IEEE J. Robot. and Automat.*, vol. 3, no. 2, 1987.

[9] Y. Nakamura, K. Nagai, and T. Yoshikawa, "Dynamics and stability in coordination of multiple robotic systems," *Int. J. Robot. Res.*, vol. 8, no. 2, Apr. 1989.

[10] J. K. Salisbury, "Whole-arm manipulation," in *Proc. 4th Int. Symp. Robot. Res.*, 1987.

[11] K. Mirza and D. E. Orin, "Force distribution for power grasp in the digits system," in *Eighth CISM-IFToMM Symp. Theory and Practice of Robots and Manipulators, (Ro.Man.Sy. '90)*, 1990.

[12] C. Melchiorri and G. Vassura, "Mechanical and control features of the University of Bologna Hand Version 2," in *Proc. 1992 IEEE/RSJ Int. Conf. Int. Robots and Syst., IROS '92*, 1992, pp. 187–193.

[13] A. Bicchi and C. Melchiorri, "Mobility and kinematic analysis of general cooperating robot systems," in *Proc. IEEE Int. Conf. Robot. and Automat.*, 1992.

[14] A. Bicchi, "Optimal control of robotic grasping," in *Proc. Amer. Cont. Conf., ACC '92*, 1992.

[15] A. A. Shabana, *Dynamics of Multibody System.* New York: Wiley, 1989.

[16] L. Nielsen, C. Canudas de Wit, and P. Hagander, "Controllability issues of robots in singular configurations," in *Proc. IEEE Conf. Robot. and Automat.*, 1991.

[17] A. Jain and G. Rodriguez, "Kinematics and dynamics of under-actuated manipulators," in *Proc. IEEE Conf. Robot. and Automat.*, 1991.

[18] J. K. Salisbury and J. J. Craig, "Articulated hands, force control and kinematic issues," *Int. J. Robot. Res.*, vol. 1, no. 1, 1982.

[19] T. Yoshikawa, "Analysis and control of robot manipulators with redundancy," in *Prep. 1st. Int. Symp. Robot. Res.*, 1983.

[20] ——, "Manipulability of robotics mechanisms," *Int. J. Robot. Res.*, vol. 4, no. 2, Summer 1985.

[21] ——, "Dynamic manipulability of robot manipulators," *J. Robot. Syst.*, vol. 2, no. 1, pp. 113–124, 1985.

[22] K. L. Doty, C. Melchiorri, and C. Bonivento, "A theory of generalized inverses applied to robotics," *Int. J. Robot. Res.*, vol. 12, no. 1, Feb. 1993.

[23] S. Lee, "Dual redundant arm configuration optimization with task-oriented dual arm manipulability," *IEEE Trans. on Robot. and Automat.*, vol. 5, no. 1, Feb. 1989.

[24] P. Chiacchio, S. Chiaverini, L. Sciavicco, and B. Siciliano, "Global task space manipulability ellipsoids for multiple-arm systems," *IEEE Trans. on Robot. and Automat.*, vol. 7, no. 5, Oct. 1991.

[25] C. Melchiorri, "Comments on 'Global task space manipulability ellipsoids for multiple-arm systems' and further considerations," *IEEE Trans. Robot. and Automat.*, vol. 9, no. 2, Apr. 1993.

[26] P. Chiacchio, S. Chiaverini, L. Sciavicco, and B. Siciliano, "Reply to comments on 'Global task space manipulability ellipsoids for multiple-arm systems' and further considerations," *IEEE Trans. Robot. and Automat.*, vol. 9, no. 2, Apr. 1993.

[27] A. Bicchi and C. Melchiorri, "Manipulability measures of cooperating arms," in *Proc. 1993 Amer. Cont. Conf., ACC '93*, 1993.

[28] G. H. Golub and C. F. VanLoan, *Matrix Computations.* Baltimore, MD: Johns Hopkins University Press, 1989.

[29] J. Baillieul, "The Nonlinear control theory of super-articulated mechanisms," in *Proc. Amer. Cont. Conf.*, 1990, pp. 2448–2451.

[30] T. Kokkinis and B. Paden, "Kinetostatic performance limits of cooperating robot manipulators using force-velocity polytopes," in *ASME Winter Annu. Meet.—Robot. Res.*, 1989.

[31] R. M. Murray and S. S. Sastry, "Grasping and manipulation using multifingered robot hands," Memo no. UCB/ERL M90/24, University of California at Berkeley, Berkeley, CA, 1990.

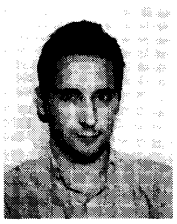

Antonio Bicchi received the Laurea degree (cum laude) from the University of Pisa in 1984, and the Ph.D. from the University of Bologna in 1988. He was a Post Doctoral Scholar at the Massachusetts Institute of Technology, Artificial Intelligence Laboratory, from 1988 to 1990.

Since 1985 he has been working at the Centro "E. Piaggio" Foundation of the University of Pisa. He is currently an Associate Researcher in Control Engineering at the Department of Electrical Systems and Automation (DSEA) of the University of Pisa, and hold teaching appointments with the University of Pisa and Siena, and with the Italian Navy's Academia. His main research interests are in the field of dexterous manipulation, including force/torque and tactile sensing and sensory control; dynamics; kinematics and control of robotic hands and legged vehicles; whole-limb robot manipulation; and nonholonomic motion planning.

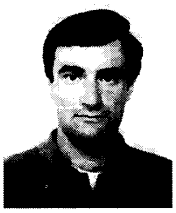

Claudio Melchiorri received the Laurea degree in electrical engineering from the University of Bologna in 1986, and the Ph.D. from the University of Bologna in 1990.

Since 1985 he has been working with DEIS, the Department of Electrical Engineering of the University of Bologna. He has been an Adjunct Associate at the University of Florida, Gainesville, FL, during 1988, and a Visiting Scientist at the Artificial Intelligence laboratory of MIT in 1990 and 1991. Currently, he is an Associate Researcher in Automatic Control at DEIS, holding a teaching appointment in Industrial Robotics. His main research interest are in the area of robotic manipulation, including topics such as dexterous hands, redundancy control, kinematics, position/force control, force/torque and tactile sensors, and in the area of digital control, including topics such as robust control and control of delay systems.

Daniele Balluchi received an electrical engineering degree from the University of Pisa in 1992. His thesis was on the analysis and control of dexterous robotic manipulation. He was granted a C.N.R. fellowship for research in nonholonomic robot motion planning.

He is cofounder and current director of DIERRE Electronics.